Facile and straightforward synthesis of superparamagnetic reduced graphene oxide–Fe_3O_4 hybrid composite by a solvothermal reaction

2013 Nanotechnology 24 025604

(http://iopscience.iop.org/0957-4484/24/2/025604)

Nanotechnology **24** (2013) 025604 (10pp) doi:10.1088/0957-4484/24/2/025604

Facile and straightforward synthesis of superparamagnetic reduced graphene oxide–Fe_3O_4 hybrid composite by a solvothermal reaction

Yue-Wen Liu[1,2], Meng-Xue Guan[1,2], Lan Feng[1,2], Shun-Liu Deng[1,2], Jian-Feng Bao[2,3], Su-Yuan Xie[1,2], Zhong Chen[2,3], Rong-Bin Huang[1,2] and Lan-Sun Zheng[1,2]

[1] Department of Chemistry, College of Chemistry and Chemical Engineering, Xiamen University, Xiamen, 361005, People's Republic of China
[2] State Key Laboratory of Physical Chemistry of Solid Surface, Xiamen University, Xiamen, 361005, People's Republic of China
[3] Department of Electronic Science, Xiamen University, Xiamen 361005, People's Republic of China

E-mail: sldeng@xmu.edu.cn

Received 19 September 2012, in final form 21 November 2012
Published 10 December 2012
Online at stacks.iop.org/Nano/24/025604

Abstract
A superparamagnetic reduced graphene oxide–Fe_3O_4 hybrid composite (rGO–Fe_3O_4) was prepared via a facile and straightforward method through the solvothermal reaction of iron (III) acetylacetonate ($Fe(acac)_3$) and graphene oxide (GO) in ethylenediamine (EDA) and water. By this method, chemical reduction of GO as well as the formation of Fe_3O_4 nanoparticles (NPs) can be achieved in one step. The Fe_3O_4 NPs are firmly deposited on the surfaces of rGO, avoiding their reassembly to graphite. The rGO sheets prevent the agglomeration of Fe_3O_4 NPs and enable a uniform dispersion of these metal oxide particles. The size distribution and coverage density of Fe_3O_4 NPs deposited on rGO can be controlled by varying the initial mass ratio of GO and iron precursor, $Fe(acac)_3$. With an initial mass ratio of GO and $Fe(acac)_3$ of 5:5, the surfaces of rGO sheets are densely covered by spherical Fe_3O_4 NPs with an average size of 19.9 nm. The magnetic-functionalized rGO hybrid exhibits a good magnetic property and the specific saturation magnetization (M_s) is 13.2 emu g^{-1}. The adsorption test of methylene blue from aqueous solution demonstrates the potential application of this rGO-Fe_3O_4 hybrid composite in removing organic dyes from polluted water.

S Online supplementary data available from stacks.iop.org/Nano/24/025604/mmedia

(Some figures may appear in colour only in the online journal)

1. Introduction

Since the initial fabrication by micro-mechanical cleavage [1], graphene, a single-atom-thick sheet of hexagonally arrayed sp^2-bonded carbon atoms, has attracted tremendous interest and shown great promise for potential applications in nanoscience and nanotechnology [2–6]. With the unique two-dimensional structure and the very high surface area [7], it has shown that graphene is an ideal substrate for the chemical deposition of many types of nanoparticles (NPs), such as metal [8, 9], metal oxide [10], quantum dots [11–14] and sulfides [15–18]. On one hand, the plate-like graphene sheet prevents the anchored NPs from agglomeration and enables their uniform dispersion while NPs separate graphene

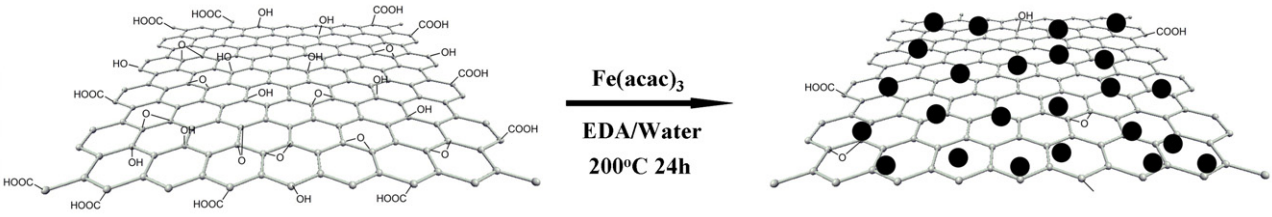

Scheme 1. Schematic illustration for the synthesis of rGO–Fe_3O_4 hybrid composite by a solvothermal reaction.

sheets and prevent their reassembly into graphite. On the other hand, the decoration of NPs will combine their desirable properties with the unprecedented properties of graphene, such as electrical [19, 20], thermal [21], and mechanical [22, 23] properties, making the as-prepared graphene-based nanocomposites promising in a variety of fields.

Currently, graphene–magnetic NPs hybrids are of great interest because of their potential applications in energy storage, enhanced optical limiting, magnetic resonance imaging (MRI), drug delivery and environmental remediation [24–28]. Among the magnetic NPs, Fe_3O_4, which exhibits good biocompatibility, strong superparamagnetism, low cost, and low toxicity, has been brought into focus. The synthesis of graphene–Fe_3O_4 (G–Fe_3O_4) hybrid nanocomposites with controlled size and coverage density of magnetic particles has long been of scientific and technological interest. The strategies for the synthesis of G–Fe_3O_4 nanocomposites can be broadly categorized into three methodologies. The first strategy involves a two-step process, in which graphene oxide (GO) generated through extensive oxidation of graphite was chemically reduced and functionalized by a surfactant or polymer, followed by the deposition of Fe_3O_4 NPs on the reduced graphene oxide (rGO) sheets [26, 29, 30]. One problem associated with the reduction of GO is that the removal of oxygen-containing groups makes rGO less hydrophilic so that it tends to aggregate in solution due to π–π stacking interactions. The introduction of surfactant or polymer can improve the dispersion of rGO in solution [31]. However, the surfactant/polymer molecules will strongly adsorb on the surface of the as-prepared nanocomposites, severely reducing their material properties. The second strategy is also a two-step process, yet the deposition of Fe_3O_4 NPs is heavily reliant on the oxidized moieties on GO sheets. For example, the iron ions were captured by carboxylate anions via coordination and precipitation by the addition of an alkaline solution, forming graphene oxide–Fe_3O_4 (GO–Fe_3O_4) hybrid composites [27, 32–34]. Through chemical reactions between oxidized moieties on GO and the functional groups on surface-modified Fe_3O_4 NPs, GO–Fe_3O_4 hybrids were also achieved [28, 35, 36] However, GO is electrically insulating and thermally unstable, seriously hindering the applications of GO–Fe_3O_4 hybrid composites. By a subsequent reduction of GO in the presence of chemical reducing agents or by heat treatment [37–41], the oxygen-containing groups of GO were removed and the GO–Fe_3O_4 hybrid could be transformed into reduced graphene oxide–Fe_3O_4 (rGO–Fe_3O_4) hybrid. However, in practical applications, some difficulties must be overcome to improve the properties and broaden the applications of the magnetic-functionalized rGO hybrid, as exemplified by the detachment of Fe_3O_4 NPs from rGO sheets after the removal of oxygen functional groups and the disruption of other parts of the hybrid during the reduction of GO. The third strategy can be classed as a 'simultaneous' methodology, in which the chemical reduction of GO and the deposition of Fe_3O_4 NPs on the carbon basal plane are combined in one single step [42–47]. This method is more efficient in preparing stable and well-dispersed rGO–Fe_3O_4 hybrid composites. However, since the synthesis was achieved by a simplified one-pot reaction, both the size distribution and the coverage density of magnetic NPs on rGO sheets were hard to control. Moreover, in the absence of binding sites on the carbon matrix, the Fe_3O_4 NPs were directly anchored on the surfaces of rGO, resulting in poor stability of the as-prepared rGO–Fe_3O_4 hybrid. A more efficient and reliable synthetic method is still desired.

Here we develop a facile and straightforward method to prepare rGO–Fe_3O_4 hybrid composites, which integrates both the electrical conductivity of graphene and the superparamagnetism of Fe_3O_4 NPs. By this method, the reduction of GO and the deposition of Fe_3O_4 NPs were simultaneously achieved by a one-pot solvothermal reaction of GO and iron (III) acetylacetonate ($Fe(acac)_3$) in ethylenediamine (EDA) and water at 200 °C, as schematically illustrated in scheme 1. In comparison with the aforementioned methods, the methodology presented in this work shows the following advantages. (1) The one-pot chemistry is facile and straightforward, in which the chemical reduction of GO and the deposition of Fe_3O_4 NPs were simultaneously completed in one single step. (2) The particle size and coverage density of Fe_3O_4 NPs on the carbon matrix are directly controlled by varying the initial mass ratio of GO and iron source, $Fe(acac)_3$. (3) The amino groups grafted on the surfaces of rGO provide extra binding sites to Fe_3O_4 NPs, promising the high stability of the as-prepared rGO–Fe_3O_4 hybrid.

2. Experimental details

2.1. Materials

Graphite was purchased from Nanjing XFNANO Materials Tech Co., Ltd (Nanjing, China). Iron (III) acetylacetonate, $Fe(acac)_3$, (98%) was purchased from J&K Scientific Co., Ltd (Beijing, China). EDA was purchased from Sinopharm

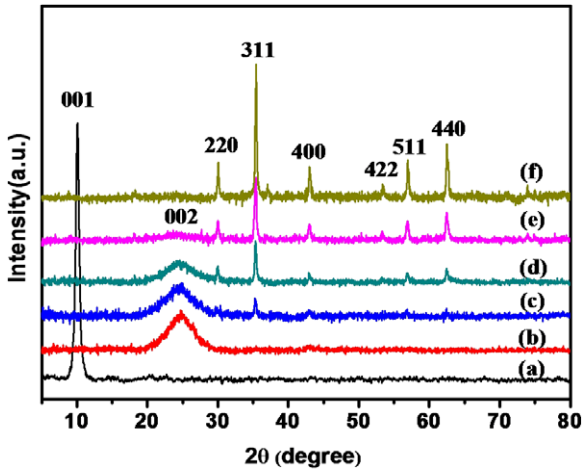

Figure 1. XRD patterns of GO (a) and the as-prepared rGO–Fe_3O_4 hybrid composites with different initial mass ratio of GO and $Fe(acac)_3$. (b) 9:1, (c) 7:3, (d) 5:5, (e) 3:7, (f) 1:9.

Chemical Reagent Co. Ltd (Shanghai, China) and was redistilled before use. All other chemicals and solvents were commercially available and used as received.

2.2. Preparation of GO

GO used in this work was synthesized via a modified Hummers method [48]. Specifically, concentrated H_2SO_4 (46 ml 98%) was slowly added to a mixture of graphite (2.0 g) and $NaNO_3$ (1.0 g) in a round-bottom flask within an ice bath. After that, $KMnO_4$ (6.0 g) was gradually added and the mixture was continuously stirred for 30 min. The ice bath was then removed and the mixture was stirred for a further 5 h. After the addition of 92 ml deionized water, the solution was stirred for 15 min and further diluted with 280 ml of deionized water. Subsequently, 10 ml H_2O_2 (30%) was added to reduce the residual $KMnO_4$. The reaction was allowed to react for 30 min, yielding a yellow solution. Then the mixture was centrifuged at 8000 rpm to collect the solid products. The obtained solid products were repeatedly dispersed in deionized water, followed by centrifugation at 8000 rpm up to 10 times to completely remove byproducts such as salts. Finally, the obtained solid was dried in a vacuum oven at 60 °C for 12 h, yielding a brown GO solid.

2.3. Synthesis of rGO–Fe_3O_4 hybrid composites via solvothermal reactions

In a typical synthesis of rGO–Fe_3O_4 hybrid, a total amount of 100 mg of GO and iron source $Fe(acac)_3$ were dispersed in 50 ml of EDA/water (in a volume ratio of 9:1) by mild sonication. Then the mixture was transferred into a Teflon-line autoclave. The autoclave was sealed and maintained at 200 °C for 24 h. After the reaction, the autoclave was cooled down to room temperature. The black solid products were collected by an external magnetic field and copiously washed with water and ethanol. When solvothermal reaction was performed with the initial mass ratio of GO to $Fe(acac)_3$ of 9:1, the obtained solid products were collected by a centrifugation method (12 000 rpm) because of the unsatisfied magnetic property.

2.4. Adsorption test of rGO–Fe_3O_4 hybrid composites towards methylene blue (MB)

Analytical grade MB was used to prepared 100 ml stock aqueous solution (0.6 mg ml^{-1}), which could be further diluted to the required concentrations. The adsorption experiments were carried out in glass vials at room temperature. Typically, 10 ml MB aqueous solution with a known concentration and 5.1 mg rGO–Fe_3O_4 hybrid composite were added into a 25 ml glass vial and then intensely stirred at room temperature for 24 h. After the removal of rGO–Fe_3O_4 composite by an external magnetic field, the equilibrium concentration of MB was measured with a UV–vis spectrometer at its maximum absorbance wavelength (664 nm).

2.5. Characterization

The sizes and morphologies of products were characterized by scanning electron microscopy (SEM, Hitachi S-4800) and transmission electron microscopy (TEM, TECNAI F-30). Powder x-ray diffraction (XRD) patterns were obtained on a X'pert PRO diffractometer with Cu Kα radiation (λ = 1.5418 Å) and a graphite monochromator from 5° to 80° at a scanning rate of 10° min^{-1}. X-ray photoelectron spectroscopy (XPS) was performed on a Quantum 2000 spectrometer, with the Al Kα line used as the excitation source. The magnetic properties of the rGO–Fe_3O_4 hybrid composite were studied with a superconducting quantum interference device (SQUID, MPMS-XL-7). The hysteresis loop of the magnetization was obtained by varying H between +15 000 and −15 000 Oe at 300 K. Ultraviolet spectroscopy was performed on a Shimadzu 2550 UV–vis spectrophotometer. Magnetic resonance imaging (MRI) experiments on GO and the magnetic rGO hybrid with concentrations increasing from 0 to 200 μg ml^{-1} in 1% agarose gel were performed on a Varian 7.0-T MRI system. An extremity coil was used for the data acquisition, using a FSE (Fast Spin Echo) sequence (TR: 5000 ms, TE: 100 ms).

3. Results and discussion

X-ray diffraction (XRD) patterns were used to investigate the phase and structure of the starting GO and the as-prepared products. As shown in figure 1(a), the XRD pattern of GO exhibits a sharp peak at 2θ = 10.1°, indicating the characteristic (001) reflection. The rGO–Fe_3O_4 hybrid composites were synthesized at 200 °C for 24 h by solvothermal method, using $Fe(acac)_3$ as iron source and EDA/water as solvent. On varying the initial mass ratio of GO and $Fe(acac)_3$, the as-prepared products display different XRD patterns. Figure 1(c) shows the representative XRD pattern of a hybrid prepared with the initial mass ratio of GO and $Fe(acac)_3$ of 7:3. It can be seen that the sharp characteristic peak of GO disappears while a broad peak at about 24.5° rises. Both the d_{002} value and the broadness of this reflection are typical for the randomly restacking of graphene sheets due to the loss of oxygen-containing

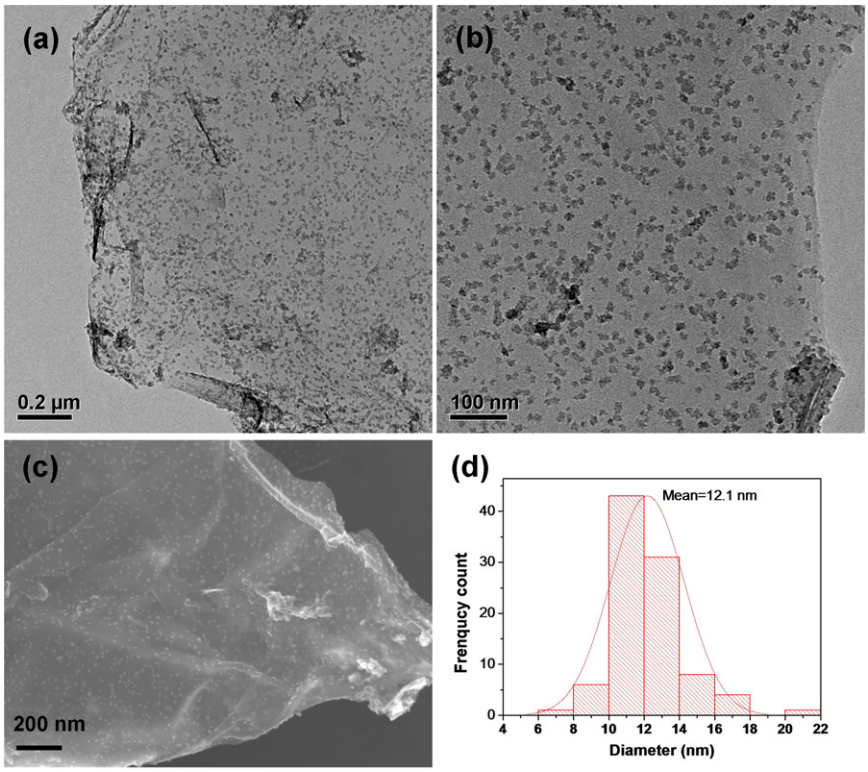

Figure 2. TEM images with different magnifications (a), (b), SEM image (c) of the rGO–Fe_3O_4 hybrid composite prepared with an initial mass ratio of GO and $Fe(acac)_3$ of 7:3, and the corresponding size distribution of Fe_3O_4 NPs on the surfaces of rGO sheets (d).

functional groups in the reaction process. The positions and relative intensities of the remaining diffraction peaks match well with the standard XRD data of cubic Fe_3O_4 (JCPDS card No. 86-1359). The observation in the XRD patterns confirms the successful deposition of Fe_3O_4 NPs on the surfaces of rGO sheets by the one-pot solvothermal reaction.

The sizes and morphologies of the as-prepared products were further studied by TEM and SEM. Figures 2(a) and (b) show representative TEM images of the rGO–Fe_3O_4 hybrid composite prepared with an initial mass ratio of GO and $Fe(acac)_3$ of 7:3. The Fe_3O_4 NPs with an average size of 12.1 nm are well decorated on the surfaces of rGO sheets, which are nearly flat and have a large area up to a micrometer scale. The distribution of magnetic NPs is uniform and no free Fe_3O_4 NPs are detected outside the range of the graphene sheets. In the representative SEM image (figure 2(c)) of this rGO–Fe_3O_4 hybrid composite, the graphene flakes exhibit a slightly wrinkled surface and the Fe_3O_4 NPs appear as bright dots. No obvious conglomeration of Fe_3O_4 NPs is observed.

XPS was also employed to analyze the starting GO and the products of solvothermal reactions. The C 1s high-resolution XPS spectrum of GO (figure 3(a)) contains four typical components, corresponding to the carbon atoms in four types of functional group: the nonoxygenated ring C (284.5 eV), the C in C–O bond (286.3 eV), the C in carbonyl (287.5 eV), and the C in carboxyl (O–C=O) (288.7 eV). This indicates a fairly high degree of oxidation was carried out during the Hummers method. After solvothermal reaction, the relative intensities of the three components associated with oxygen-containing functional groups decrease markedly, suggesting that most of the oxygen functional groups have been successfully removed (figure 3(b)). Moreover, the deoxygenation of GO was also found to be accompanied by nitrogen incorporation from the reaction solvent (EDA). As seen in figure 3(d), a N 1s peak of amino groups at about 400 eV appears in the XPS survey scan spectrum of rGO–Fe_3O_4 hybrid composite. In the C 1s XPS spectrum (figure 3(b)), the additional peak is correlated with the C in the C–N bonds. The nucleophilic substitution reactions between surface-exposed epoxy groups on GO sheets and EDA account for the surface amination, as explained in detail below [49, 50]. The amino groups grafted on rGO surfaces show great promise in the Fe_3O_4 NPs engineering process. In the Fe 2p high-resolution XPS spectrum (figure 3(c)), the binding energies at 711.2 eV and 724.8 eV are related to Fe $2p_{3/2}$ and Fe $2p_{1/2}$, respectively, which are very close to the values of Fe_3O_4 published in the literature [43, 51, 52]. It is noteworthy that no charge transfer satellite of Fe $2p_{3/2}$ at about 720 eV is detected, indicating the formation of mixed oxides of Fe(II) and Fe(III), such as Fe_3O_4 [51].

The above characterizations demonstrate the high efficiency of our solvothermal method in the synthesis of rGO–Fe_3O_4 hybrid composite. In order to investigate the controllability and flexibility of this method on the size and density distribution of Fe_3O_4 NPs on graphene sheets, parallel experiments were conducted by changing the reaction parameters, such as the initial feed ratio of reagents, the reaction temperature, and the reaction time. It is found that the initial mass ratio of GO and iron source $Fe(acac)_3$ in the synthesis process is essential in controlling the size

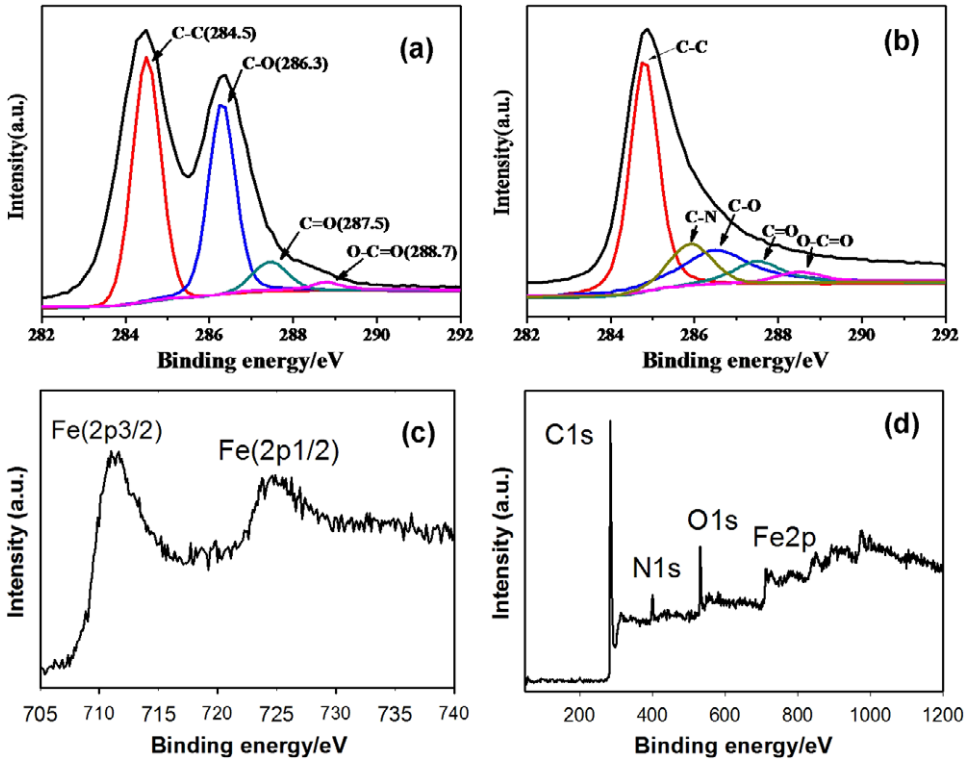

Figure 3. High-resolution XPS spectrum of C 1s of GO (a), high-resolution XPS spectra of C 1s (b), Fe 2p (c) and survey scan (d) of the rGO–Fe_3O_4 hybrid composite prepared with an initial mass ratio of GO and $Fe(acac)_3$ of 7:3.

distribution of Fe_3O_4 NPs and their coverage density on the surfaces of rGO.

As shown in figure 1, at a fixed reaction temperature (200 °C) and fixed reaction time (24 h), when the initial mass ratio of GO to $Fe(acac)_3$ was varied from 7:3 to 5:5, 3:7 and 1:9, the intensities of Fe_3O_4 diffraction peaks become more and more distinct (figures 1(c)–(f)), mainly due to the increasing coverage of Fe_3O_4 NPs on graphene sheets. Simultaneously, the (002) peak corresponding to the rGO tends weaken gradually and cannot be detected for the hybrid which was prepared with the initial mass ratio of GO and $Fe(acac)_3$ of 1:9 (figure 1(f)). This result suggests that the graphene sheets can no longer stack with each other to form a crystalline structure when the coverage of Fe_3O_4 NPs is dense enough. On the other hand, when the mass ratio of GO to $Fe(acac)_3$ was varied from 7:3 to 9:1, the diffraction peaks of Fe_3O_4 become too weak to detect (figure 1(b)), indicating a very small amount of Fe_3O_4 NPs were formed and decorated on graphene sheets in this condition.

Figures 4(a) and (b) show representative TEM images of rGO–Fe_3O_4 hybrid composite prepared at fixed reaction temperature (200 °C) and fixed reaction time (24 h), while the mass ratio of GO and $Fe(acac)_3$ was altered from 7:3 to 5:5. It is concluded that the size of Fe_3O_4 NPs and the coverage density of Fe_3O_4 NPs on graphene sheets are obviously increased, which is consistent with the observation in the XRD pattern (figure 1(d)). The surfaces of rGO are densely covered by spherical Fe_3O_4 NPs with an average size of 19.9 nm. In addition, the distribution of magnetic particles remains monodispersed and uniform. No obvious vacancy on graphene sheets is observed. Despite the high coverage of NPs on the surfaces of rGO (close to saturation), the sheets remain flat, and no curled or crumpled sheets are observed. As measured from the high-resolution TEM (HRTEM) image (inset in figure 4(b)), the lattice fringe spacing between two adjacent crystal planes of the particle is 0.29 nm, corresponding to the (220) lattice plane of a cubic structure of Fe_3O_4. In the SEM image (figure 4(c)), the Fe_3O_4 NPs are firmly deposited on the surfaces of rGO with larger size and higher density than that obtained with the initial mass ratio of GO and $Fe(acac)_3$ of 7:3.

When the initial mass ratio of GO and $Fe(acac)_3$ was further changed to 3:7 and 1:9, the size of Fe_3O_4 particles was found to be considerably larger than that obtained with mass ratio of GO and $Fe(acac)_3$ of 7:3 and 5:5. Additionally, obvious agglomeration of Fe_3O_4 is observed, as shown in figures 5(a) and (b). This result is reasonable because more $Fe(acac)_3$ will generate more Fe_3O_4 to increase both the size and number of Fe_3O_4 particles. However, as shown in figures 4(a) and (b), when the initial mass ratio of GO and $Fe(acac)_3$ is 5:5, the surfaces of graphene sheets are very close to saturation. As the number and size of Fe_3O_4 particles increase, the formed particles undergo aggregation on graphene sheets because of the lack of deposition place. These results further confirm the important role of the graphene surface in the preparation of rGO–Fe_3O_4 hybrid, in which the plate-like carbon basal plane prevents the deposited Fe_3O_4 NPs from agglomeration and enable their uniform dispersion. In fact, when the decomposition of $Fe(acac)_3$ was conducted in similar conditions excluding the addition of GO,

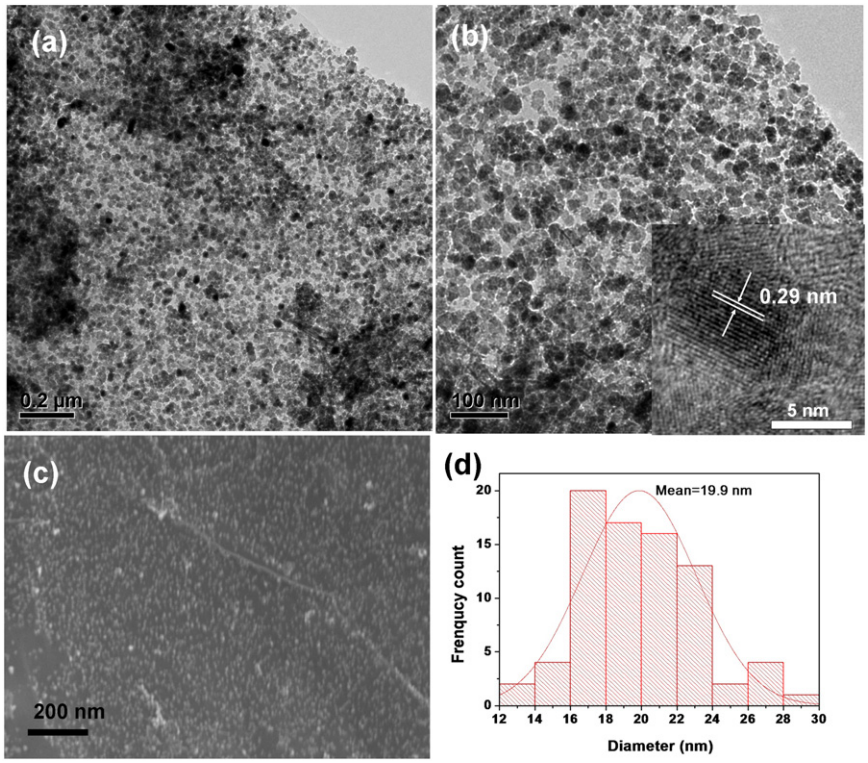

Figure 4. TEM images with different magnification (a), (b), SEM image (c) of rGO–Fe_3O_4 hybrid composite prepared with the initial mass ratio of GO and $Fe(acac)_3$ of 5:5, and the corresponding size distribution of Fe_3O_4 NPs on the surfaces of rGO sheets (d). The inset in (b) shows the HRTEM image of Fe_3O_4 NPs.

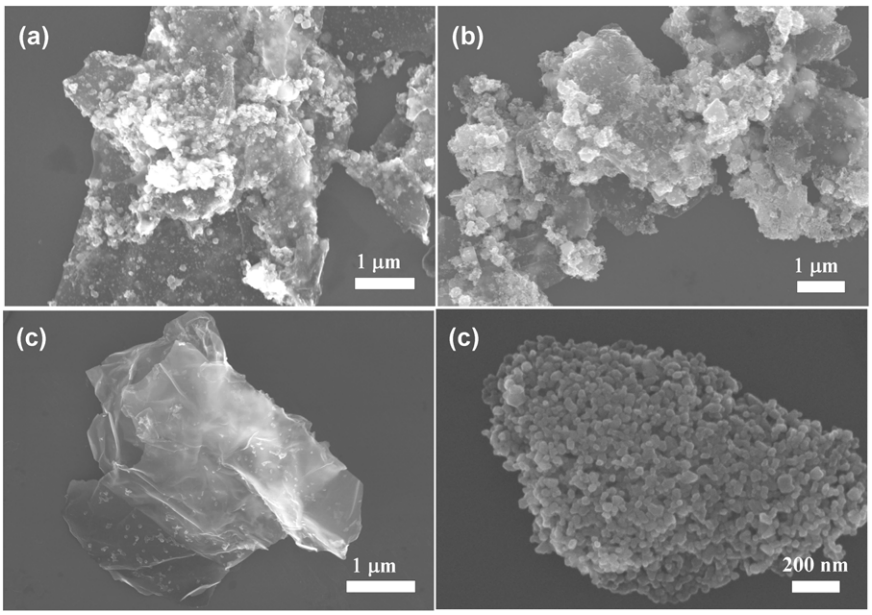

Figure 5. SEM images of rGO–Fe_3O_4 hybrid composites prepared with the initial mass ratio of GO and $Fe(acac)_3$ of 3:7 (a), 1:9 (b), 9:1 (c), aggregated Fe_3O_4 NPs prepared from the controlled experiment excluding the addition of GO (d).

severe aggregation was found for the formed Fe_3O_4 NPs (figure 5(d)). When the initial mass ratio of GO and $Fe(acac)_3$ was changed to 9:1, only a small amount of Fe_3O_4 particles with irregular shape were deposited on the surfaces of the graphene sheets (figure 5(c)).

According to the above analysis, it is concluded that not only were the crystallized Fe_3O_4 NPs effectively deposited on the reduced graphene sheets through the high-temperature decomposition of $Fe(acac)_3$ but also the particle size and coverage density could be successfully controlled by tuning

the initial mass ratio of the reagents. It is known that the particle size and size distribution are extremely important for revealing the size-dependent properties of magnetic materials. In our process, GO and $Fe(acac)_3$ are firstly dispersed in EDA/water by mild sonication, in which the iron precursors are adsorbed on the surface of GO through the interaction with oxygen-containing groups on GO sheet. The coverage density of Fe_3O_4 NPs on the rGO surface increases with increasing feed ratio of $Fe(acac)_3$. This is likely due to the elevated concentration of $Fe(acac)_3$ increasing the amount of iron precursor adsorbed on the surface of GO. In addition, when the total mass of reactants is kept fixed (100 mg in this work) while the iron precursor amount is increased, the available GO surface is decreased. This further leads to an increasing number of iron precursor on each GO sheet. At the beginning of the solvothermal process, the pyrolysis of iron precursor $Fe(acac)_3$ generates a large number of monomers which are believed to be active atomic or molecular iron species via a series of complicated decomposition reactions and redox reactions. As the concentration of monomer exceeds the critical concentration, the monomers undergo aggregation to form nuclei (clusters). Finally, after the burst-nucleation process, the monomer concentration decreases, and the nuclei gradually grow into Fe_3O_4 nanocrystals with the consumption of monomer [53–55]. At higher concentrations of $Fe(acac)_3$, more iron precursors are adsorbed on the surface of GO. In the subsequent solvothermal process, the burst-nucleation and crystal growth mechanism have resulted in a higher coverage density of Fe_3O_4 NPs on the surface of rGO, while the Ostwald ripening of smaller particles accounts for the formation of larger particles.

During the reaction process, the oxygen-containing groups of GO, such as hydroxyl, carbonyl, epoxy and carboxylic groups, were lost by heat treatment. Meanwhile, as demonstrated in the literature, the deoxygenation of GO was also related to the reduction ability of EDA to GO [56]. In fact, the EDA used in the solvothermal reaction has another important role apart from its solvent role and reducibility to GO: on account of the surface-exposed epoxy groups, the surface modification of GO by EDA takes place easily through the corresponding nucleophilic substitution reaction [49, 50, 56]. In this way, the EDA molecules were chemically grafted to the GO surfaces by the formation of C–N bonds, which is consistent with XPS analysis. The combination of chemical reduction and surface modification of GO is of particular importance in producing novel graphene-based composites. In this study, the amino groups in EDA grafted on rGO surfaces show great promise in the Fe_3O_4 NPs engineering process. The magnetic NPs are firmly decorated on the surface of rGO. The bonding in the rGO–Fe_3O_4 hybrid is believed to involve covalent interactions between NH_2 groups of EDA and Fe_3O_4 particles as well as van der Waals interactions.

The decomposition of iron precursor $Fe(acac)_3$ at high temperature has been widely used in the synthesis of iron oxide NPs [54, 57]. In such process, polymeric or surfactant stabilizers play an important role in controlling the formation and morphology of magnetic NPs. However, due to the large specific surface area, the reduced GO has a particular advantage in loading magnetic NPs, effectively preventing the agglomeration of magnetic NPs and enabling their uniform dispersion. Moreover, the amino groups introduced by the nucleophilic substitution reaction of EDA and epoxy groups on GO surfaces provide extra binding sites to Fe_3O_4 NPs, which further increases the stability of rGO–Fe_3O_4 hybrid nanocomposites.

To verify the function of amino groups in the formation of rGO–Fe_3O_4 hybrid, hydrazine-reduced GO [37] rather than GO was used as starting material in the controlled experiment. As shown in figure S1(a) (available at stacks.iop.org/Nano/24/025604/mmedia), only few Fe_3O_4 NPs were found randomly deposited on the surfaces of rGO sheets. It is reasonable, because most of the oxygen-containing functional groups including epoxy groups have been removed from the surfaces of GO in the hydrazine reducing process. Therefore, the surface amination through the reaction of EDA and epoxy groups was obviously less in the solvothermal process. It is disadvantageous for the deposition of Fe_3O_4 NPs. Conversely, when EDA-reduced GO which has demonstrated the surface amination [56] was used as starting material, the surfaces of rGO were obviously covered by magnetic particles (figure S1(b) available at stacks.iop.org/Nano/24/025604/mmedia).

In order to reveal the influence of reaction time and reaction temperature on the formation of rGO–Fe_3O_4 hybrid composites, time- and temperature-dependent controlled experiments were performed with a fixed initial mass ratio of GO and $Fe(acac)_3$ of 5:5. As shown in figure S2(a) (available at stacks.iop.org/Nano/24/025604/mmedia), at 200 °C with the reduced reaction time of 0.5 h, the surfaces of rGO sheets were uniformly covered with a large number of monodispersed magnetic particles. This result means that the formation of Fe_3O_4 NPs is a quick process and can be completed within 0.5 h at 200 °C. When the decomposition of $Fe(acac)_3$ was performed at lower temperatures for 24 h, such as 120 and 150 °C, the surfaces of rGO sheets show similar deposition compared with that at 200 °C (figures S2(b) and (c) available at stacks.iop.org/Nano/24/025604/mmedia). However, the deposited Fe_3O_4 NPs exhibit poor crystallization, as shown in figure S2(d) (available at stacks.iop.org/Nano/24/025604/mmedia), with the low-intensity diffraction peaks of magnetite in the XRD patterns. Moreover, as verified by the remained diffraction peaks at 12°–13°, the reduction of GO is not complete under these conditions.

The magnetization curve of rGO–Fe_3O_4 hybrid composite prepared with an initial mass ratio of GO and $Fe(acac)_3$ of 5:5 was measured at 300 K, as shown in figure 6(a). It can be seen that the magnetic hysteresis loop shows a typical S-like curve, where the magnetic remanence is nearly zero. This reveals that there is almost no remaining magnetization when the external magnetic field is removed, suggesting that the obtained rGO–Fe_3O_4 hybrid composite exhibits a superparamagnetic behavior at room temperature. The saturation magnetization is 13.2 emu g^{-1}, which is smaller than the reported value of bulk Fe_3O_4 of 92 emu g^{-1} [58]. This can be attributed to the smaller particle size of Fe_3O_4 in the as-prepared composite. However, as demonstrated in figure 6(b), the rGO

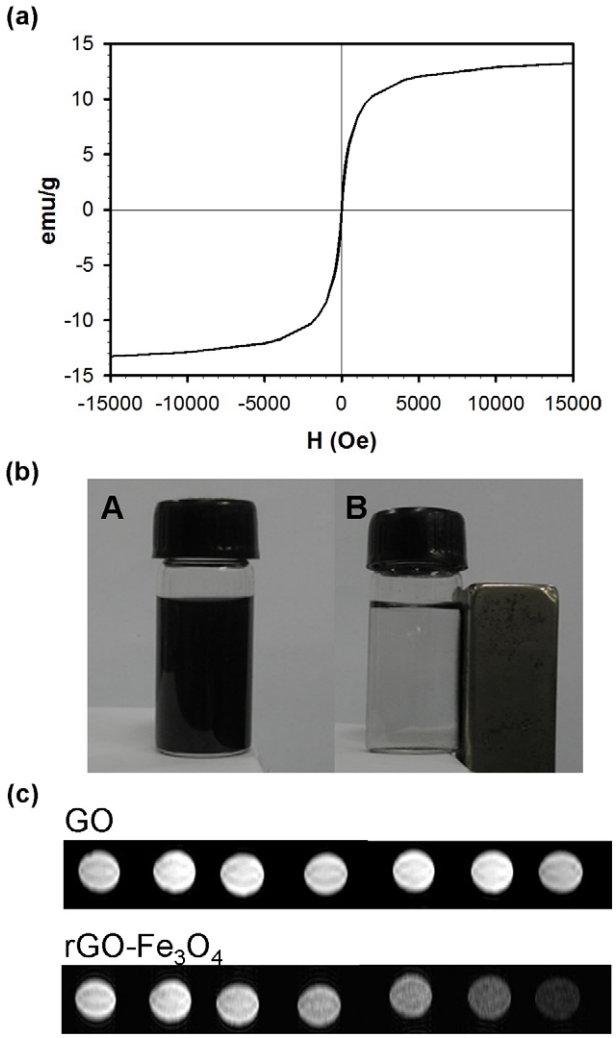

Figure 6. Magnetic hysteresis loop of rGO–Fe_3O_4 hybrid composite prepared with the initial mass ratio of GO and $Fe(acac)_3$ of 5:5 (a), photographs of the rGO–Fe_3O_4 composite dispersion in ethanol after sonication and its good response to a magnet (b), T_2-weighed MRI of GO (upper) and the rGO–Fe_3O_4 composite (lower) at different concentrations in 1% agarose gel (c) (increasing from left to right in each row: 0, 6.25, 12.5, 25, 50, 100, 200 μg ml^{-1}).

hybrid composite exhibits a good response to an external magnet. Due to the excellent magnetic property, T_2-weight MRI of the magnetic-functionalized rGO hybrid was performed and compared with that of GO. As shown in figure 6(c), no concentration-dependent enhancement of contrast was observed for the GO. However, as the concentration of the hybrid increases, contrast enhancement is obviously observed.

The adsorption test of dye MB from aqueous solution by the obtained rGO–Fe_3O_4 hybrid composite was studied by UV spectra at 664 nm. The adsorption amount of MB on rGO–Fe_3O_4 hybrid was investigated in different initial MB concentrations with respect to the same amount of rGO–Fe_3O_4 hybrid which was prepared with an initial mass ratio of GO and $Fe(acac)_3$ of 5:5. As shown in figure S3 (available at stacks.iop.org/Nano/24/025604/mmedia), the saturated adsorption amount of MB on rGO–Fe_3O_4 hybrid is about 16.2 mg g^{-1}. It is known that the π–π stacking interaction between graphene sheet and MB plays an important role in the adsorption of MB [59, 60]. The high loading density of Fe_3O_4 on rGO sheets (figure 4) may account for the relatively small adsorption of MB, since the surface area of rGO has obviously been occupied by Fe_3O_4 NPs.

4. Conclusion

In summary, we have developed a facile and straightforward method to prepare rGO–Fe_3O_4 hybrid composites through solvothermal reaction of $Fe(acac)_3$ precursor and GO in EDA and water. The particle size and coverage density of Fe_3O_4 NPs on the reduced graphene sheets can be controlled by varying the initial mass ratio of GO and $Fe(acac)_3$. With an initial mass ratio of GO and $Fe(acac)_3$ of 5:5, the surfaces of rGO are densely covered by spherical Fe_3O_4 NPs with an average size of 19.9 nm. The obtained rGO–Fe_3O_4 hybrid shows a superparamagnetic property and can be removed by the force of external magnetic field. Thus, the graphene-based magnetic nanocomposites, with excellent magnetic property and high surface area, are expected to find practical applications in various areas such as biomaterials and environmental remediation.

Acknowledgments

This work was supported by the National Key Basic Research Program of China (2013CB933901), the National Natural Science Foundation of China (Nos 21171140, 21021061, 21031004, U1205111), the Fundamental Research Funds for the Central Universities (Nos 2011121013, 2012121020) and NFFTBS (No. J1030415).

References

[1] Novoselov K S, Geim A K, Morozov S V, Jiang D, Zhang Y, Dubonos S V, Grigorieva I V and Firsov A A 2004 Electric field effect in atomically thin carbon films *Science* **306** 666–9
[2] Fowler J D, Allen M J, Tung V C, Yang Y, Kaner R B and Weiller B H 2009 Practical chemical sensors from chemically derived graphene *ACS Nano* **3** 301–6
[3] Yoo E, Kim J, Hosono E, Zhou H-S, Kudo T and Honma I 2008 Large reversible Li storage of graphene nanosheet families for use in rechargeable lithium ion batteries *Nano Lett.* **8** 2277–82
[4] Stankovich S, Dikin D A, Dommett G H B, Kohlhaas K M, Zimney E J, Stach E A, Piner R D, Nguyen S T and Ruoff R S 2006 Graphene-based composite materials *Nature* **442** 282–6
[5] Wu Q, Xu Y, Yao Z, Liu A and Shi G 2010 Supercapacitors based on flexible graphene/polyaniline nanofiber composite films *ACS Nano* **4** 1963–70
[6] Qu L, Liu Y, Baek J-B and Dai L 2010 Nitrogen-doped graphene as efficient metal-free electrocatalyst for oxygen reduction in fuel cells *ACS Nano* **4** 1321–6
[7] Stoller M D, Park S, Zhu Y, An J and Ruoff R S 2008 Graphene-based ultracapacitors *Nano Lett.* **8** 3498–502

[8] Yang J, Tian C, Wang L and Fu H 2011 An effective strategy for small-sized and highly-dispersed palladium nanoparticles supported on graphene with excellent performance for formic acid oxidation *J. Mater. Chem.* **21** 3384–90

[9] Chen X, Wu G, Chen J, Chen X, Xie Z and Wang X 2011 Synthesis of 'clean' and well-dispersive Pd nanoparticles with excellent electrocatalytic property on graphene oxide *J. Am. Chem. Soc.* **133** 3693–5

[10] Chang H, Sun Z, Ho K Y-F, Tao X, Yan F, Kwok W-M and Zheng Z 2011 A highly sensitive ultraviolet sensor based on a facile *in situ* solution-grown ZnO nanorod/graphene heterostructure *Nanoscale* **3** 258–64

[11] Li L-L, Liu K-P, Yang G-H, Wang C-M, Zhang J-R and Zhu J-J 2011 Fabrication of graphene–quantum dots composites for sensitive electrogenerated chemiluminescence immunosensing *Adv. Funct. Mater.* **21** 869–78

[12] Tu W, Wang W, Lei J, Deng S and Ju H 2012 Chemiluminescence excited photoelectrochemistry using graphene–quantum dots nanocomposite for biosensing *Chem. Commun.* **48** 6535–7

[13] Chen J, Xu F, Wu J, Qasim K, Zhou Y, Lei W, Sun L-T and Zhang Y 2012 Flexible photovoltaic cells based on a graphene–CdSe quantum dot nanocomposite *Nanoscale* **4** 441–3

[14] Yan J, Ye Q, Wang X, Yu B and Zhou F 2012 CdS/CdSe quantum dot co-sensitized graphene nanocomposites via polymer brush templated synthesis for potential photovoltaic applications *Nanoscale* **4** 2109–16

[15] Zhao X, Zhou S, Jiang L-P, Hou W, Shen Q and Zhu J-J 2012 Graphene–CdS nanocomposites: facile one-step synthesis and enhanced photoelectrochemical cytosensing *Chem. Eur. J.* **18** 4974–81

[16] Jiang Z, Wang C, Du G, Zhong Y J and Jiang J Z 2012 *In situ* synthesis of SnS_2@graphene nanocomposites for rechargeable lithium batteries *J. Mater. Chem.* **22** 9494–6

[17] Wang B, Park J, Su D, Wang C, Ahn H and Wang G 2012 Solvothermal synthesis of CoS_2–graphene nanocomposite material for high-performance supercapacitors *J. Mater. Chem.* **22** 15750–6

[18] Pan S and Liu X 2012 ZnS–graphene nanocomposite: synthesis, characterization and optical properties *J. Solid State Chem.* **191** 51–6

[19] Novoselov K S, Jiang Z, Zhang Y, Morozov S V, Stormer H L, Zeitler U, Maan J C, Boebinger G S, Kim P and Geim A K 2007 Room-temperature quantum Hall effect in graphene *Science* **315** 1379

[20] Zhang Y, Tan Y-W, Stormer H L and Kim P 2005 Experimental observation of the quantum Hall effect and Berry's phase in graphene *Nature* **438** 201–4

[21] Balandin A A, Ghosh S, Bao W, Calizo I, Teweldebrhan D, Miao F and Lau C N 2008 Superior thermal conductivity of single-layer graphene *Nano Lett.* **8** 902–7

[22] Lee C, Wei X, Kysar J W and Hone J 2008 Measurement of the elastic properties and intrinsic strength of monolayer graphene *Science* **321** 385–8

[23] Booth T J *et al* 2008 Macroscopic graphene membranes and their extraordinary stiffness *Nano Lett.* **8** 2442–6

[24] Li B, Cao H, Shao J, Qu M and Warner J H 2011 Superparamagnetic Fe_3O_4 nanocrystals@graphene composites for energy storage devices *J. Mater. Chem.* **21** 5069–75

[25] Zhang X, Yang X, Ma Y, Huang Y and Chen Y 2010 Coordination of graphene oxide with Fe_3O_4 nanoparticles and its enhanced optical limiting property *J. Nanosci. Nanotechnol.* **10** 2984–7

[26] Cong H-P, He J-J, Lu Y and Yu S-H 2010 Water-soluble magnetic-functionalized reduced graphene oxide sheets: *in situ* synthesis and magnetic resonance imaging applications *Small* **6** 169–73

[27] Yang X, Zhang X, Ma Y, Huang Y, Wang Y and Chen Y 2009 Superparamagnetic graphene oxide–Fe_3O_4 nanoparticles hybrid for controlled targeted drug carriers *J. Mater. Chem.* **19** 2710–4

[28] Xie G, Xi P, Liu H, Chen F, Huang L, Shi Y, Hou F, Zeng Z, Shao C and Wang J 2011 A facile chemical method to produce superparamagnetic graphene oxide–Fe_3O_4 hybrid composite and its application in the removal of dyes from aqueous solution *J. Mater. Chem.* **22** 1033–9

[29] Zhang Y, Chen B, Zhang L, Huang J, Chen F, Yang Z, Yao J and Zhang Z 2011 Controlled assembly of Fe_3O_4 magnetic nanoparticles on graphene oxide *Nanoscale* **3** 1446–50

[30] Zhu G, Liu Y, Xu Z, Jiang T, Zhang C, Li X and Qi G 2010 Flexible magnetic nanoparticles-reduced graphene oxide composite membranes formed by self-assembly in solution *ChemPhysChem* **11** 2432–7

[31] Stankovich S, Piner R D, Chen X, Wu N, Nguyen S T and Ruoff R S 2006 Stable aqueous dispersions of graphitic nanoplatelets via the reduction of exfoliated graphite oxide in the presence of poly(sodium 4-styrenesulfonate) *J. Mater. Chem.* **16** 155–8

[32] Ji L, Tan Z, Kuykendall T R, Aloni S, Xun S, Lin E, Battaglia V and Zhang Y 2011 Fe_3O_4 nanoparticle-integrated graphene sheets for high-performance half and full lithium ion cells *Phys. Chem. Chem. Phys.* **13** 7170–7

[33] Chandra V, Park J, Chun Y, Lee J W, Hwang I-C and Kim K S 2010 Water-dispersible magnetite-reduced graphene oxide composites for arsenic removal *ACS Nano* **4** 3979–86

[34] Yao Y, Miao S, Liu S, Ma L P, Sun H and Wang S 2012 Synthesis, characterization, and adsorption properties of magnetic Fe_3O_4@graphene nanocomposite *Chem. Eng. J.* **184** 326–32

[35] He F, Fan J, Ma D, Zhang L, Leung C and Chan H L 2010 The attachment of Fe_3O_4 nanoparticles to graphene oxide by covalent bonding *Carbon* **48** 3139–44

[36] Liang J, Xu Y, Sui D, Zhang L, Huang Y, Ma Y, Li F and Chen Y 2010 Flexible, magnetic, and electrically conductive graphene/Fe_3O_4 paper and its application for magnetic-controlled switches *J. Phys. Chem.* C **114** 17465–71

[37] Stankovich S, Dikin D A, Piner R D, Kohlhaas K A, Kleinhammes A, Jia Y, Wu Y, Nguyen S T and Ruoff R S 2007 Synthesis of graphene-based nanosheets via chemical reduction of exfoliated graphite oxide *Carbon* **45** 1558–65

[38] Fan X, Peng W, Li Y, Li X, Wang S, Zhang G and Zhang F 2008 Deoxygenation of exfoliated graphite oxide under alkaline conditions: a green route to graphene preparation *Adv. Mater.* **20** 4490–3

[39] Shin H-J *et al* 2009 Efficient reduction of graphite oxide by sodium borohydride and its effect on electrical conductance *Adv. Funct. Mater.* **19** 1987–92

[40] Becerril H A, Mao J, Liu Z, Stoltenberg R M, Bao Z and Chen Y 2008 Evaluation of solution-processed reduced graphene oxide films as transparent conductors *ACS Nano* **2** 463–70

[41] Wang X, Zhi L and Muellen K 2008 Transparent, conductive graphene electrodes for dye-sensitized solar cells *Nano Lett.* **8** 323–7

[42] Su J, Cao M, Ren L and Hu C 2011 Fe_3O_4–graphene nanocomposites with improved lithium storage and magnetism properties *J. Phys. Chem.* C **115** 14469–77

[43] He H and Gao C 2010 Supraparamagnetic, conductive, and processable multifunctional graphene nanosheets coated with high-density Fe_3O_4 nanoparticles *ACS Appl. Mater. Interfaces* **2** 3201–10

[44] Shi W *et al* 2011 Achieving high specific charge capacitances in Fe_3O_4/reduced graphene oxide nanocomposites *J. Mater. Chem.* **21** 3422–7
[45] Shen X, Wu J, Bai S and Zhou H 2010 One-pot solvothermal syntheses and magnetic properties of graphene-based magnetic nanocomposites *J. Alloys Compounds* **506** 136–40
[46] Shen J, Hu Y, Shi M, Li N, Ma H and Ye M 2010 One step synthesis of graphene oxide-magnetic nanoparticle composite *J. Phys. Chem.* C **114** 1498–503
[47] Zhou K, Zhu Y, Yang X and Li C 2010 One-pot preparation of graphene/Fe_3O_4 composites by a solvothermal reaction *New J. Chem.* **34** 2950–5
[48] Hummers W S Jr and Offeman R E 1958 Preparation of graphitic oxide *J. Am. Chem. Soc.* **80** 1339
[49] Bourlinos A B, Gournis D, Petridis D, Szabo T, Szeri A and Dekany I 2003 Graphite oxide: chemical reduction to graphite and surface modification with primary aliphatic amines and amino acids *Langmuir* **19** 6050–5
[50] Lerf A, He H, Forster M and Klinowski J 1998 Structure of graphite oxide revisited *J. Phys. Chem.* B **102** 4477–82
[51] Morel A-L *et al* 2008 Sonochemical approach to the synthesis of Fe_3O_4@SiO_2 core–shell nanoparticles with tunable properties *ACS Nano* **2** 847–56
[52] Teng X, Black D, Watkins N J, Gao Y and Yang H 2003 Platinum–maghemite core–shell nanoparticles using a sequential synthesis *Nano Lett.* **3** 261–4
[53] Qiao R, Yang C and Gao M 2009 Superparamagnetic iron oxide nanoparticles: from preparations to *in vivo* MRI applications *J. Mater. Chem.* **19** 6274–93
[54] Sun S and Zeng H 2002 Size-controlled synthesis of magnetite nanoparticles *J. Am. Chem. Soc.* **124** 8204–5
[55] Ren T, Si Y, Yang J, Ding B, Yang X, Hong F and Yu J 2012 Polyacrylonitrile/polybenzoxazine-based Fe_3O_4@carbon nanofibers: hierarchical porous structure and magnetic adsorption property *J. Mater. Chem.* **22** 15919–27
[56] Che J, Shen L and Xiao Y 2010 A new approach to fabricate graphene nanosheets in organic medium: combination of reduction and dispersion *J. Mater. Chem.* **20** 1722–7
[57] Liang X, Ji G, Zhang L, Yang Y and Liu X 2011 Synthesis and properties of Fe_3O_4 nanoparticles by solvothermal method using iron(III) acetylacetonate *Glass Phys. Chem.* **37** 459–65
[58] Popplewell J and Sakhnini L 1995 The dependence of the physical and magnetic-properties of magnetic fluids on particle-size *J. Magn. Magn. Mater.* **149** 72–8
[59] Xie L, Ling X, Fang Y, Zhang J and Liu Z 2009 Graphene as a substrate to suppress fluorescence in resonance Raman spectroscopy *J. Am. Chem. Soc.* **131** 9890–1
[60] Li F, Bao Y, Chai J, Zhang Q, Han D and Niu L 2010 Synthesis and application of widely soluble graphene sheets *Langmuir* **26** 12314–20